Hindawi
Advances in Civil Engineering
Volume 2024, Article ID 4166203, 15 pages
https://doi.org/10.1155/2024/4166203

Research Article

A Comparison Study of Edge Line Estimation Algorithms for Dimensional Quality Assessment of Precast Concrete Slabs

Chang-Yong Yi,[1] **Fangxin Li**,[2,3] **Julian Pratama Putra Thedja**,[3,4] **Sung-Han Sim**,[3] **Yoon-Ki Choi**,[5] **Geon Hwee Kim**,[6] **and Min-Koo Kim**[7]

[1]*Intelligent Construction Automation Center, Kyungpook National University, 80 Daehak-ro, Buk-gu, Daegu 41566, Republic of Korea*
[2]*Business School, Hohai University, Nanjing, China*
[3]*School of Civil, Architectural Engineering and Landscape Architecture, Sungkyunkwan University, Suwon 16419, Republic of Korea*
[4]*PT Miyamoto International Indonesia, Jakarta, Indonesia*
[5]*Earth Turbine, 36, Dongdeok-ro 40-gil, Jung-gu, Daegu 41905, Republic of Korea*
[6]*School of Mechanical Engineering, Chungbuk National University, Cheongju, Chungbuk 28644, Republic of Korea*
[7]*Department of Architectural Engineering, Chungbuk National University, Cheongju, Chungbuk 28644, Republic of Korea*

Correspondence should be addressed to Min-Koo Kim; joekim@chungbuk.ac.kr

Received 7 September 2023; Revised 22 December 2023; Accepted 27 December 2023; Published 24 January 2024

Academic Editor: Jorge Branco

Point cloud data-based edge line extraction is an important task for accurate geometrical inspection of precast concrete (PC) elements in the construction industry. Although a few edge extraction algorithms have been developed so far based on point cloud data, little attention has been paid on which edge extraction algorithm performs the best in terms of edge estimation accuracy. To tackle the research gap, this study aims to evaluate currently available edge extraction algorithms in order to determine optimal algorithm for precise geometrical inspection of PC elements. To do this, simulated scan points are first generated and used for algorithm performance analysis using a geometrical model and a measurement noise modeling that determine the coordinates of simulated scan points. For validation of the simulation approach, comparison tests with experimental data are performed and the results show that the simulation approach has a high similarity of more than 90% compared to experimental data in terms of the number of scan points, scan pattern, and scan density, proving the effectiveness of the simulation-based evaluation method. In addition, it shows that a least square regression (LSR) algorithm provides the best performance with an edge extraction accuracy of 1.56 and 2.71 mm for simulated and experimental scan points, respectively. The contributions of this study are (1) development of the geometrical model and noise modeling based on actual scan data and (2) validation of simulated-based evaluation method on the lab-scale PC slabs.

1. Introduction

Computer vision technologies have been widely applied in various industries for automation and enhancement of productivity [1–3]. This trend is not exceptional in the construction industry, with techniques like prefabricated construction and offsite manufacturing popularly utilized in recent years [3, 4]. One example is the quality control of precast concrete (PC) elements including precast girders and precast concrete slabs during the manufacturing stage [4–8]. However, one critical issue related to quality control is that failure in assembly between PC elements often occurs onsite during the construction stage [9, 10]. To tackle the problem, accurate dimensional quality assessment of individual component is necessary since large dimensional errors can cause structural failures and construction delays [11–13]. Due to their excellent accuracy and speed, noncontact sensing tools, point cloud data obtained from laser scanners have been widely utilized for dimensional quality assessment (DQA) of PC elements owing to their high accuracy and speed [14–20].

In general, the construction tolerance standards possess an important role in assuring the dimensional quality for PC

Table 1: Dimensional Tolerance for Precast and Prestressed Concrete Elements [21, 22].

Feature	Dimensional attribute (tolerance)
Dimension	Length (±6 mm); width (±6 mm); thickness (±6 mm)
Position	Length (horizontal (±6 mm); vertical (±6 mm))
Straightness	Size (±10 mm)
Squareness	Size (±3 mm)

elements. Table 1 summarized the dimensional tolerance for prefabrication elements based on the inspection checklists from Precast Concrete Institute [21] and American Concrete Institute [22]. There are four dimensional features needed to check in the geometry category, which are dimension, position, straightness, and squareness. Each dimensional feature consists of specific checklists for inspection called "dimensional attribute." For instance, length and vertical are the attributes for the feature "Position." It is necessary to guarantee each dimensional attribute falls within its specified tolerance.

Some studies used scan points obtained from laser scanning to extract edge lines for DQA of prefabricated construction components [23, 24]. However, few studies have focused on the edge line extraction algorithm that performs best among them to ensure accurate DQA of PC elements. Moreover, collecting actual scan points for the evaluation of edge line estimation algorithms under varying scan parameters is time-consuming because of the heavy workloads caused by the experimental setup. Therefore, to tackle these problems, this study proposes a simulation-based evaluation approach to determine optimal edge line extraction algorithm for DQA of PC slabs with rectangular shapes. To this end, simulated scan points were created by developing a mathematical relationship between the scanner and the target object with respect to the principle of laser beam emission. Thus, the optimal edge extraction algorithm and scan parameters can be determined without actual scans, resulting in an efficient scan configuration determination. For validation, this study conducts a comparison test with an experiment-based evaluation method that collected actual scan points.

There are two reasons to utilize the simulation-based method instead of directly using actual scan data. First, the simulation-based method offers better efficiency as there is no need for data collection in field. Second, more in-depth analysis is available in the simulation-based method since a variety of scan parameters including incidence angle and scan density can be tested to verify the relationship between accuracy and each parameter. The uniquenesses of this study are as follows: (1) development of a geometrical model with noise modeling that determines the coordinates of scan points falling on target surfaces and (2) validation of the proposed method with experiment data under varying scanning parameters to ensure accurate and efficient DQA.

This article is structured as follows. Relevant previous studies are presented and analyzed in detail in Section 2. Section 3 describes the simulation method that generates virtual scan points using the geometrical model, followed by in-depth validation of the method in Sections 4 and 5. Sections 6 and 7 present the discussion points and a short summary of the findings of this study.

2. Literature Review

2.1. DQA Based on Laser Scanning. Numerous studies have suggested employing DQA through the utilization of laser scanning on building elements, including steel-frame structures [25, 26], building facades [27, 28], timber beams [29], and precast bridge slabs [30]. For example, Bosche et al. [25, 26] proposed an object detection method that recognizes construction components from point cloud data for dimensional compliance inspection of a steel-frame structure. In this study, the as-designed model and the acquired data from laser scanning were registered together to extract the construction components, resulting in automatic DQA with respect to the dimensional tolerance. Truong-Hong et al. [27] detected the building boundary points of windows and doors from laser scanner data and transformed these data into a solid model to extract the as-is dimensions. In this work, experimental tests revealed that there was an average discrepancy of 1.2% (about 15 mm) for three different building facades between the ground truth measurements and the extracted dimensions. Subsequently, Truong-Hong et al. [28] proposed a new feature recognition method that integrates an angle criterion and voxelization to reconstruct the building models from laser scanner data for dimensional compliance control. The experimental tests showed that the proposed approach recognized building boundaries and features with an error of 0.6%. Caballero et al. [29] proposed a dimensional estimation algorithm for the cross-sectional contour of timber beams based on point cloud data. The collected scan points falling on the beams were first separated into numerous slices, and then, the dimensions of the beams were extracted based on an alpha-shape algorithm. The validation tests on timber beams provided a relative dimensional error of 3%. Yoon et al. [30] also presented an optimal placement method for assembling precast bridge slabs based on laserscanner data. The as-built dimensions of dimensional features on the girders were first extracted to guide the placement of the precast deck panels. Field tests indicated that 54 mismatches could be addressed by implementing the proposed method.

In summary, although numerous studies on laser scanning–based DQA of construction components have been comprehensively studied and developed, few studies have focused on which edge extraction algorithm performs best to ensure accurate DQA of PC elements. Thus, it is necessary to assess existing edge extraction algorithms under different scan parameters to determine an optimal algorithm with scan configurations for the accurate geometrical inspection of PC elements.

2.2. Edge Line Extraction Algorithms for DQA. This section describes the existing edge extraction algorithms that use point cloud data in detail. In this study, three primary algorithms using point cloud data [31–34] are used for performance analysis. First, the concept of the vector sum algorithm [31] is explained in Figure 1. The algorithm was proposed using a unique geometrical formation of point cloud data, with respect to the assumption that the pattern of the scan points is regular. It employs the

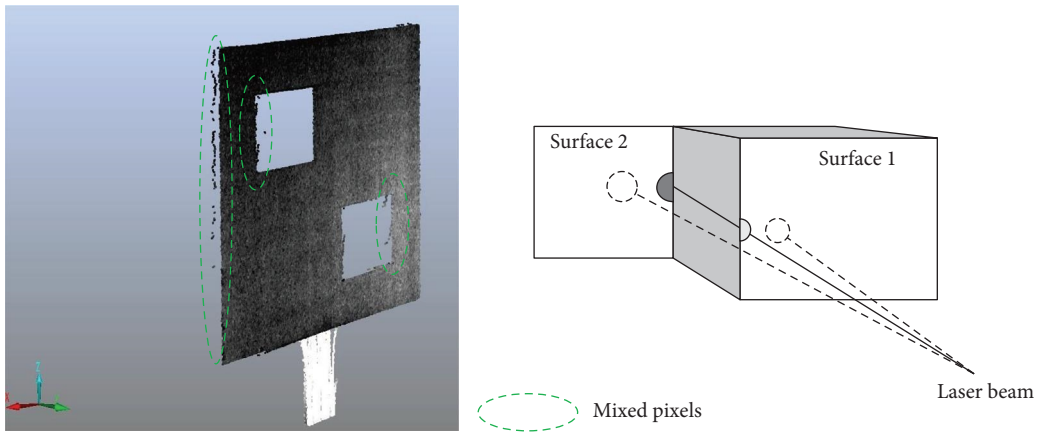

FIGURE 1: Mixed-pixel phenomenon. The phenomenon appears at the edges of a construction object where the beam is separated into two and reflected from two varying surfaces.

addition of eight vectors $V(p_i)$ from a scanning point (p_i) toward its eight nearest adjacent scanning points $p_{i^m m=1\ldots8}$ to serve as a marker for identifying edge points. If the eight vectors' sum $V(p_i)$ of a target point (p_i) is smaller or equal to 2.5 times of the interval of the scan points (D), the target point (p_i) is recognized as a nonedge point. Alternatively, if not, the target point (p_i) is classified as an edge point. After isolating the edge points, a least-squares fitting algorithm was employed to fit each edge line. Finally, dimensional compensation for the edge loss of the target construction object is conducted using the model developed by Tang et al. [35] to address the mixed-pixel phenomenon. Figure 1(a) shows the mixed-pixel effect that occurs as one beam is separated into two and falls on varying surfaces at varying ranges from the laser scanner. Figure 1(b) indicates an example of mixed pixels caused by the edges, and the laser scanner detects a combination of two distinct signals, leading to imprecise measurements of the point cloud data.

Next, the other two edge extraction algorithms using the LSR algorithm [32] and the RANSAC algorithm [34] are illustrated in Figure 2. The concepts of the "LSR1" and "LSR2" algorithms proposed by Wang et al. [33] and Fischler and Bolles [34] are based on the generation of hypothesis scan points. Here, the two LSR algorithms (LSR1 and LSR2) are the same in the fitting method but different in the data sets used. As can be seen in Figure 2, the data set used for the LSR1 regards the mixed pixel points as hypothesis scan points to be used for edge line fitting. In contrast, the LSR2 algorithm ignores the mixed pixel scan points but instead generates background points outside the true edges of the PC slab to be used as hypothesis scan points. The initial step of both algorithms involves the extraction of last valid scan points (LVSPs) located within the edge lines. Following this, hypothesis scan points (HSPs) are generated next to the LVSPs. Ultimately, the centers located between the LVSPs' and HSPs' center points are computed. These centers are then employed in a least-square regression process to establish an edge line. It is important to note that the centers of the respective laser beams are identified as the center points of both LVSPs and HSPs.

The other fitting algorithm investigated in this research is the RANSAC algorithm [33, 34] which is a popular algorithm for line fitting due to its high capability in accurately fitting scan points even in the presence of numerous outliers. The two algorithms, RANSAC1 and RANSAC2, have a similar line fitting principle to the LSR1 and LSR2 algorithms that use virtual scan points. The two RANSCAN algorithms are different each other in terms of the use of mixed pixel scan data for line fitting.

3. Methodology

3.1. Overview. Figure 3 shows the schematic of the proposed simulation-based evaluation method. First, the simulated scan points were generated using a geometrical model with a noise modeling for evaluation of edge extraction algorithms. Then, the experimental scan points were collected, and data preprocessing was performed on the acquired scan points to validate the geometric model. Finally, the five edge line algorithms of vector-sum algorithm, "LSR1," "LSR2," "RANSAC1," and "RANSAC2" were performed on both simulated scan points and experimental scan points to calculate DQA accuracy for evaluation of edge extraction algorithms. Illustration of each step is provided in the subsequent sections.

3.2. Generation of Simulated Scan Points Using Geometrical Model. There are three steps for generation of simulated scan points: (1) creation of a geometrical model to identify scan points' coordinates falling on target surfaces, (2) modeling of measurement noise, and (3) generation of simulated scan points on PC elements.

Step 1—development of a geometrical model: Figure 4 presents the geometrical model of a target surface. Note that the scan parameters from the technical instruction of the laser scanner is assumed to be precise and reliable. Applying the laser scanner's line-of-sight principle, the y-coordinate of the laser beam can be calculated on the target surface with a horizontal angle of H and a vertical angle of V as follows:

$$y = d \times \frac{1}{\cos H} \times \tan V = d \times \frac{1}{\cos(\Delta H \times i)} \times \tan(\Delta V \times j) \quad (1)$$

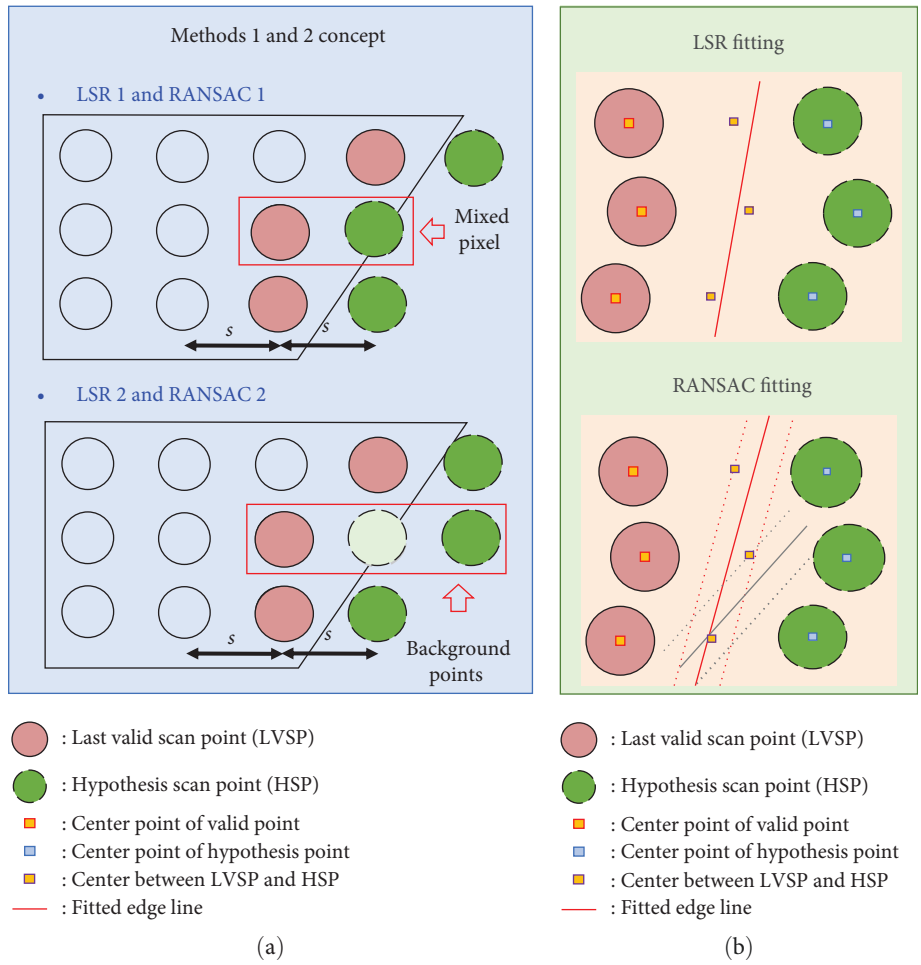

Figure 2: Data sets and working principle of edge line fitting for the algorithms of "LSR1," "LSR2," "RANSAC1," and "RANSAC2": (a) data sets used for edge line fitting; (b) working principle of edge line fitting algorithms.

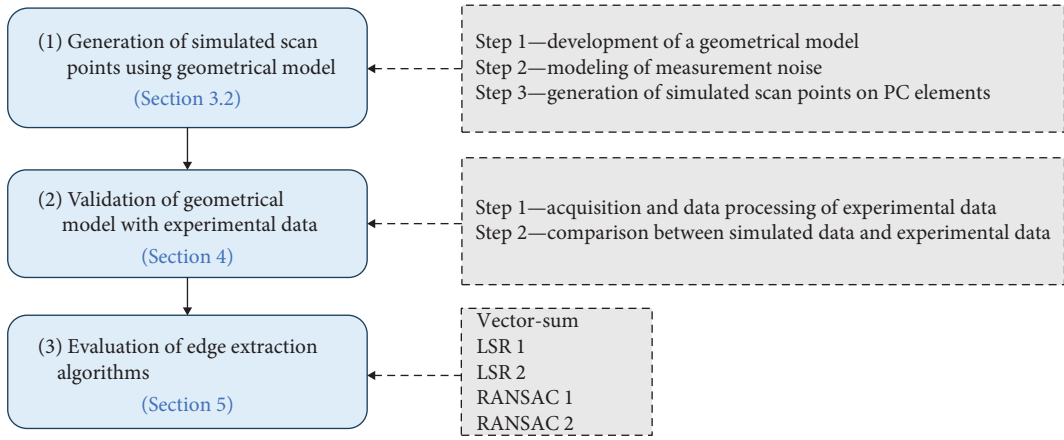

Figure 3: Overall procedure for the proposed simulation-based evaluation method.

where respectively, H and V stand for the horizontal and vertical angular resolution. The vertical scanning distance (d) between the surface of the object and the laser scanner is represented. The following equation is used to calculate the laser beam's x coordinate under the same horizontal and vertical angles (H and V), similar to how the y coordinate is calculated:

$$x = d \times \frac{1}{\cos V} \times \tan H = d \times \frac{1}{\cos(\Delta V \times j)} \times \tan(\Delta H \times i) \quad (2)$$

Step 2—modeling of measurement noise: This step aims to reflect the actual position of each scan point with

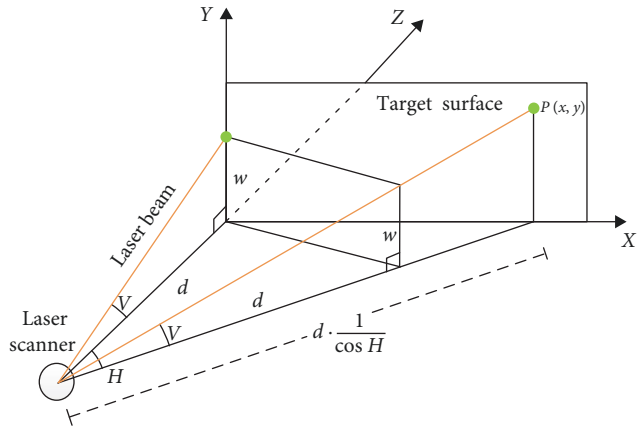

FIGURE 4: Geometrical model that determines the x and y coordinates of a laser point.

measurement noise. Here, the measurement noise is defined as the standard deviation of the distance values of scan points from the best-fit plane generated to the scan points. An empirical method of modeling the measurement noise of a laser scanner is developed, which can be adapted to other types of laser scanners. Figure 5(a) shows the flowchart for modeling the measurement noise. There are three substeps of modeling the measurement noise. Substep 1—collecting "multiple" base scan data sets with different scanning geometry and calculating its measurement noises for each set. First, "multiple" base scan data sets with varying scan distances and incident angles are collected, and its measurement noise for each set is calculated. Figure 5(b) shows the test setup for collection of base scan sets for measurement noise modeling. Here, the best-fit plane generated about the scan points is computed using the least square algorithm. Then, the measurement noise is determined as the average perpendicular distances from the scan points to the fitted plane. Figure 5(c) shows the measurement noise with increasing scan distances and incident angles, which were calculated using the multiple base scan data sets. Substep 2—creation of scan points using the geometrical model. The scan points are first created using the geometrical model. Note that all the created scan points have different scan distances and incident angles so the measurement noise for each scan point needs to be estimated based on the base scan data sets collected in Substep 1. Substep 3—selection of two closest base scan data sets to each created scan point. For each scan point created using the geometrical model, the two closest base scan data sets to each scan point of the created scan set are determined for measurement noise estimation. Substep 4—do interpolation of the measurement noise for each created scan point. Measurement noise for each created scan point is performed by interpolating the measurement noises of the selected two base scan data sets.

Step 3—generation of simulated scan points on PC elements: Figure 6 shows the generation of the simulated scan points on the surfaces of PC elements using the geometrical model and noise modeling. The geometrical model of Equations (1) and (2) was used to create the initial scan points with the laser scanner placed above the center of the PC element, respectively. Then, the measurement noise is added to each created scan point based on the proposed model in Step 2. Here, the region including the area of the as-designed PC element was set as the region of interest by having a margin with a user-defined value of h. In simulation, each scan point has its center coordinate with a radius indicating the circle size. If the center position or the circle edge of a scan point is located outside the outer edge of the as-designed PC element, the scan point is removed based on the coordinate information of the scan. For the scan points inside shear pockets, they are also removed in the same way. For this process, the circle size (D_L) of the created scan points was calculated using Equation (3)

$$D_L = D_0 + \text{abs}(\text{L} - \text{L}_0)\alpha_{\text{D}}, \tag{3}$$

where L_0 is the distance from the laser scanner's focal point to the target surface, and L is the perpendicular distance between the laser scanner and the target surface. D_0 and α_D are the diameter of the laser beam and the divergence rate when emitting the laser beam, respectively.

4. Validation of Geometrical Model with Experimental Data

This step aims to validate the geometrical model with experimental data. There are two steps for the validation: (1) acquisition and data processing of experiment data and (2) comparison between the simulation and experimental data.

Step 1—acquisition and data processing of experiment data: The experimental scan points were first collected from a laboratory test. Figure 7 shows the experimental configuration. A lab-scaled specimen as shown in Figure 7(a) was chosen for DQA accuracy evaluation because the dimensions of the well-made lab-scaled specimen can be measured accurately at the level of less than one-millimeter error. Figure 7(b) shows the dimensions of the specimen which are 1,000 mm (length) × 400 mm (width) × 150 mm (depth). There are six shear keys and four shear pockets on the top surface of the PC slab. The dimensions of the shear pockets are 130 mm × 70 mm, while the dimensions of the six shear keys are 60 mm × 50 mm. For data collection, a terrestrial laser scanner, FARO S70, was used. With the consideration of the constraints of the scanning area, the scanner was positioned at a height of 2 m above the center of the top surface of the PC slab. Also note that the scanner was held by a framework. Figure 7(c) shows a photo illustrating the test configuration, and two flat mirrors were used to collect side surface scan points. In this research, two angular resolutions, namely, 0.072° and 0.036°, were chosen to examine the impact of scan density. Note that these two parameters are commonly selected to examine the impact of scan density for lab-scale construction components. In addition, two different incident angles of 0° and 45° were used to investigate the effect of the incident angle

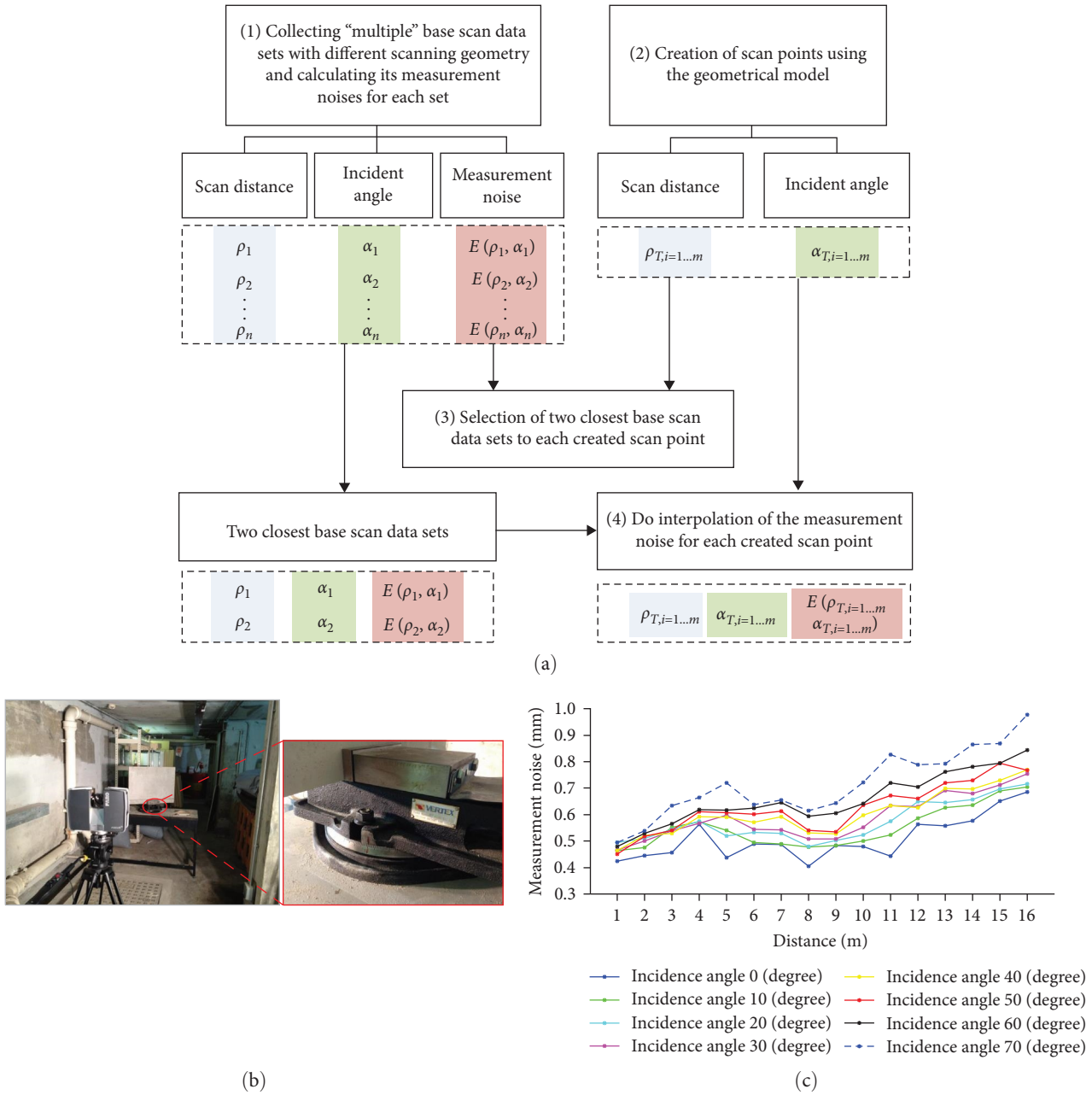

Figure 5: Modeling of the measurement noise: (a) process of modeling the measurement noise; (b) test setup for collection of base scan sets for measurement noise modeling; and (c) measurement noise with increasing scan distances and incident angles.

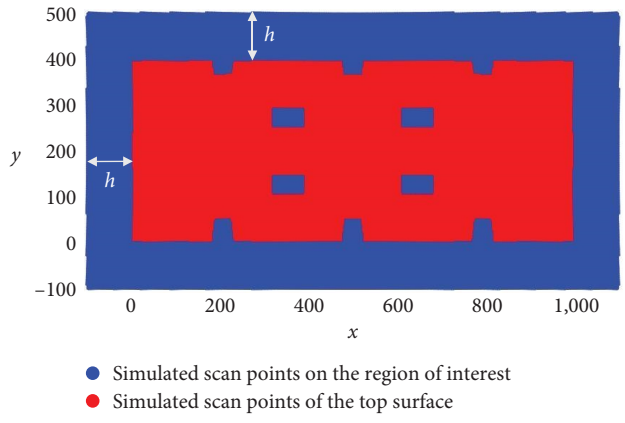

Figure 6: Simulated scan point generation using the geometrical model.

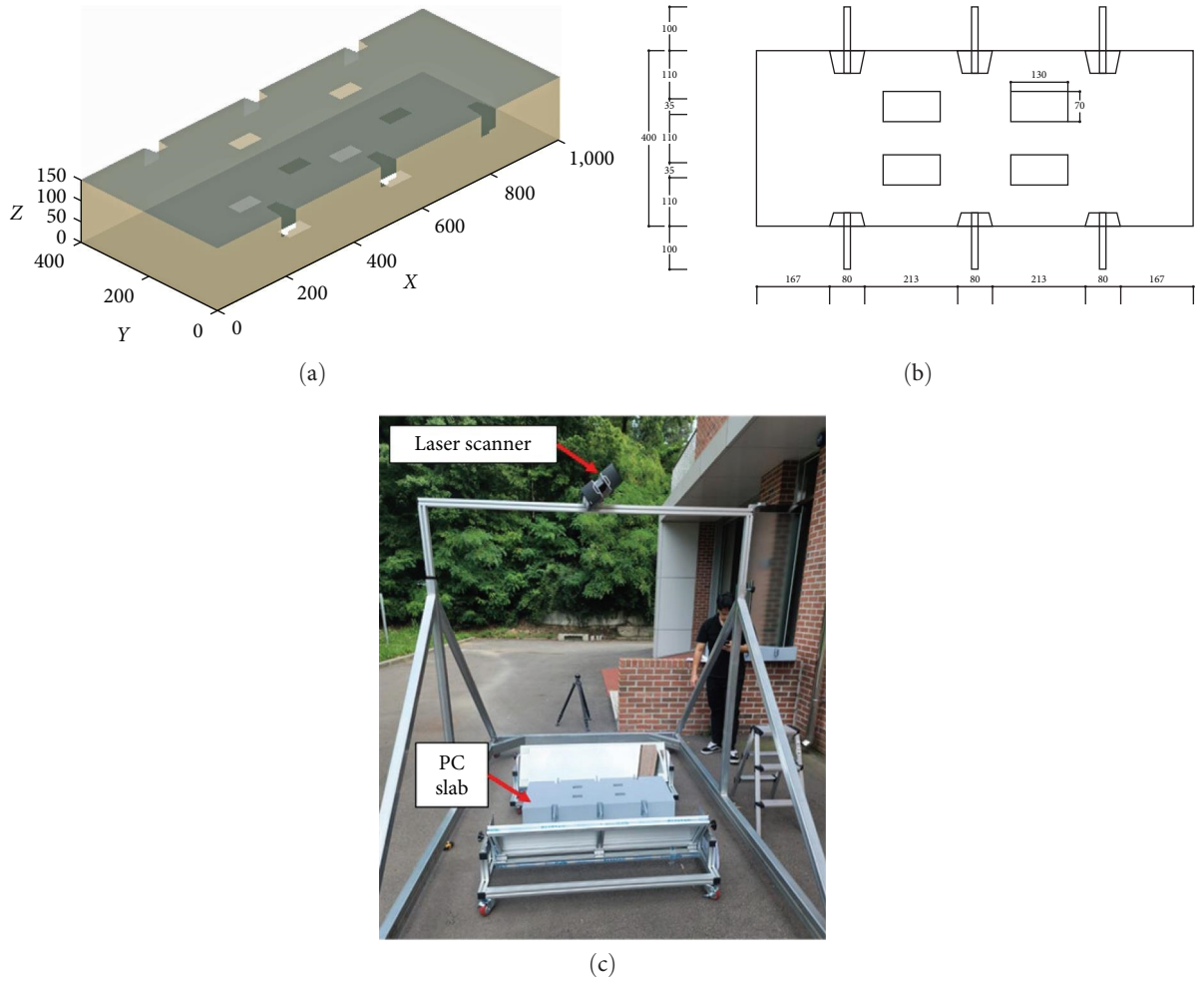

Figure 7: Experimental configuration: (a) 3D model of the lab-scale PC slab; (b) dimensions; and (c) experimental setup with flat mirrors.

on the DQA results of the side surfaces. This is because that these two incident angles are easy to be adjusted by rotating the mirror angles.

Figure 8 presents the data processing results aiming to separate the top surface scan points from the raw scan data involving noise data. First, a density-based clustering algorithm called DBSCAN algorithm [36] was used. Figure 8(a) shows the outcome of the implementation of the algorithm. Since this study assumes that the largest cluster among the raw scan points is the top surface scan points, the scan points from the top surface were extracted by the DBSCAN algorithm as shown in Figure 8(b). However, there were unnecessary scan points corresponding to steel rebars embedded in the PC element's side surfaces. In order to remove the rebar scan points, the RANSAC algorithm was employed in this study. Figure 8(c) shows the recognition results of rebar scan points, while Figure 8(d) shows only the scan points of the top surface after removing the rebar-associated scan points. Regarding the use of DBSCAN algorithm, a trial-and-error approach was adopted in this study in order to carefully select the two input parameters of the DBSCAN algorithm including "Eps" and "MinPts." Figure 9(a) illustrates the definitions of each input parameter and how different values for "MinPts" and "Eps" affect the segmentation results. Following a series of trial-and-error tests, the values of 6 and 9 mm were chosen for "MinPts" and "Eps" to extract the scan points from the top surface of the PC element, respectively. As can be seen in Figure 9(b), it was found that difference cases with inappropriate value selection for "Eps" and "MinPts" cause the overextraction or less-extraction problems.

Step 2—comparison between simulated data and experimental data: For validation, the simulated scan points were compared to the experimental scan points in terms of (1) scan pattern, (2) scan density, and (3) number of scan points. Figure 10 shows scan patterns between simulation and experiment. According to the laser scanner's vertical and horizontal scans, row and column information is used to create each scan point. Figure 10(a) shows a comparison of scan patterns in columns. The column pattern indicates how and where the laser beams are positioned along the longitudinal direction. The column pattern marks the scan points in the same column with the same color, whereas the row pattern assigns the same color to the scan points in the same row. Two patterns between the simulation and experiment are very similar from the left hand to the right hand. Figure 10(b) shows a comparison of scan patterns in the rows. It is observed that

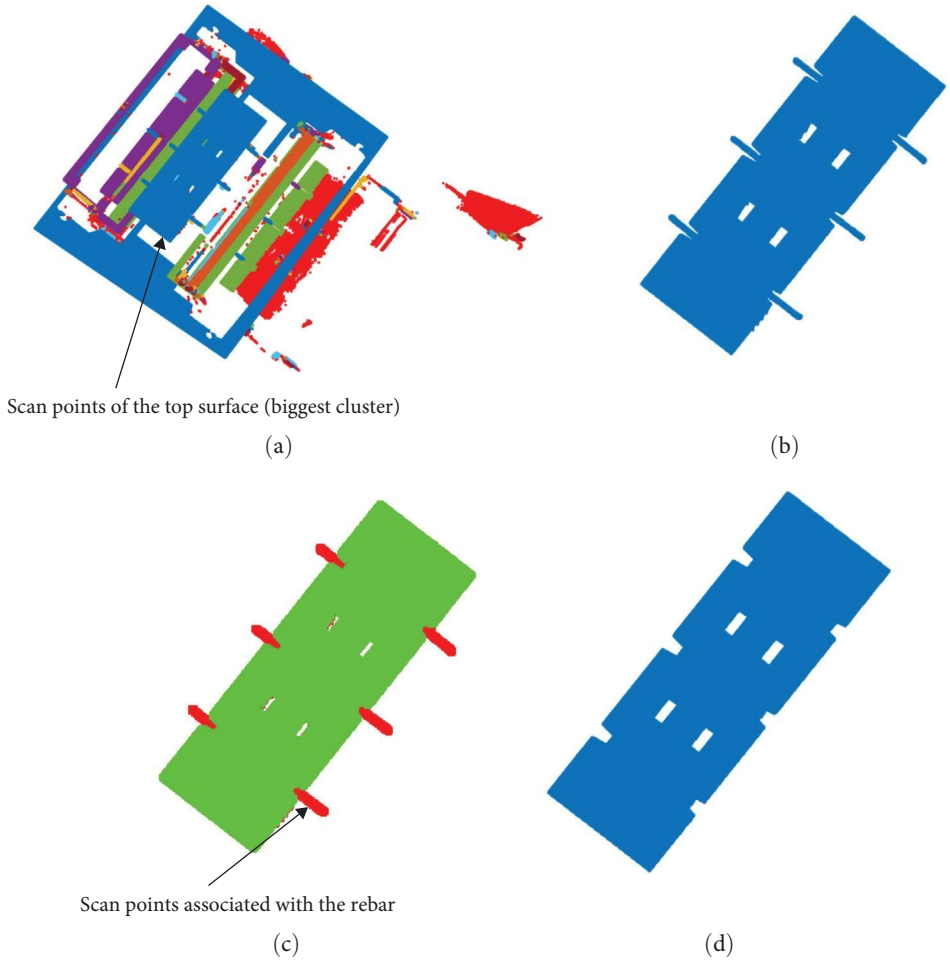

Figure 8: The results of data processing: (a) DBSCAN implementation results on the raw scan points; (b) extraction of top surface scan points from the PC element while excluding noises; (c) RANSAC implementation results on the top surface scan points; and (d) top surface scan points after the scan points of the rebars have been removed.

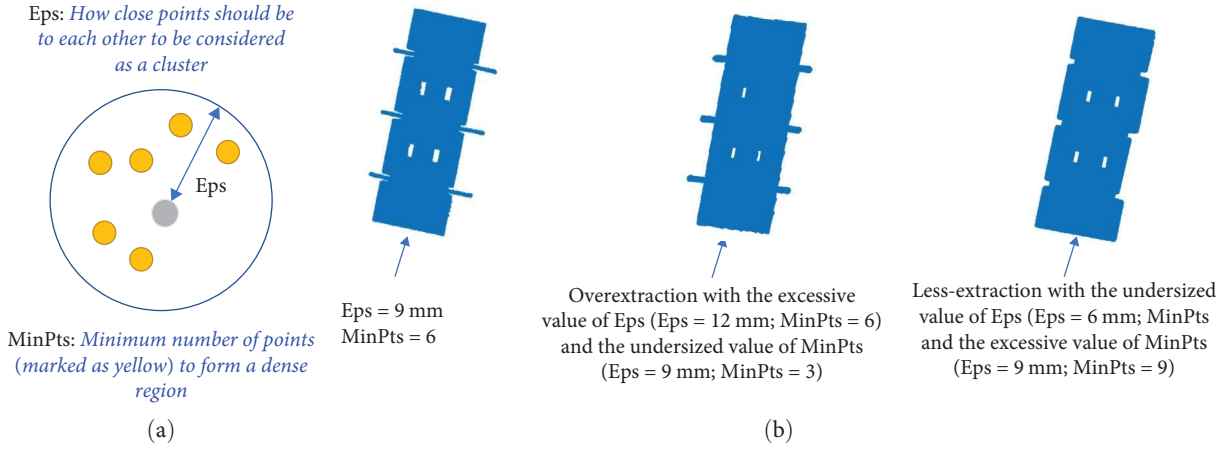

Figure 9: Selection of input parameters of the DBSCAN algorithm for extraction of scan points of the top surface of the PC element. (a) Definitions of the "MinPts" and "Eps" and (b) extraction results with different values of "MinPts" and "Eps".

the patterns are also well matched although the experimental pattern shows slightly curved lines.

Next, the scan density and number of scan points were calculated. Table 2 shows the discrepancies in terms of scan density and number of scan points between the scan points from simulation and experiment. The average discrepancy of number of scan points was 4.2%, ranging from 0.58% to 7.99%. A maximum average discrepancy of 7.99% was

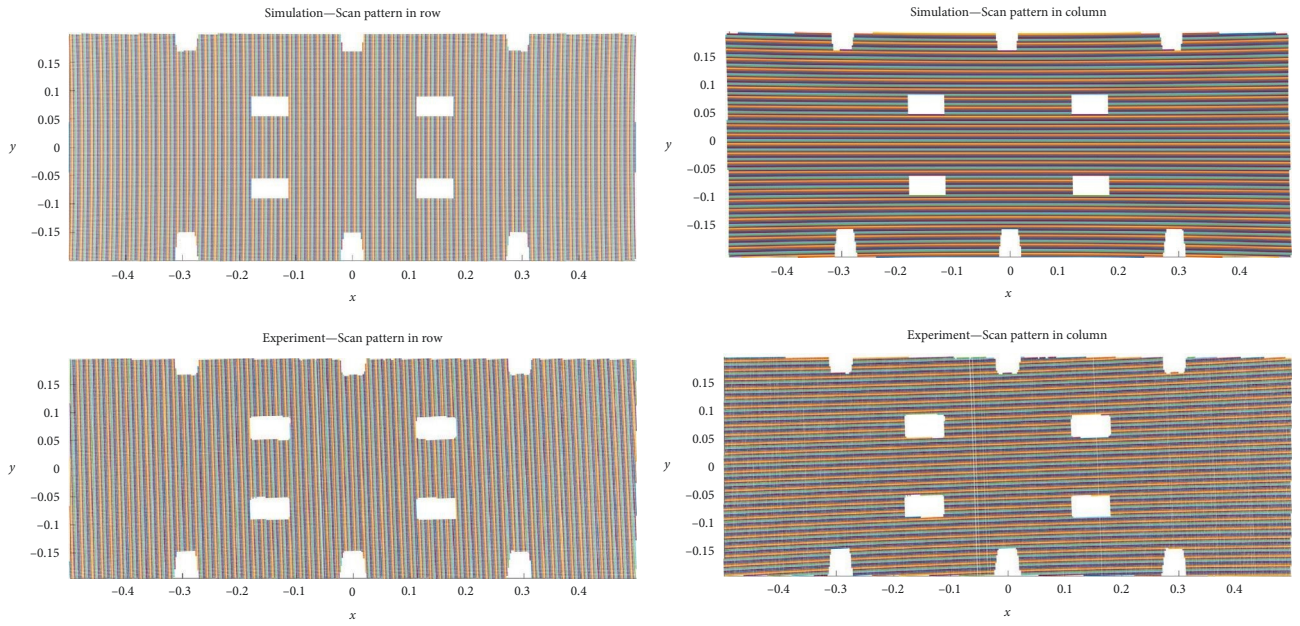

Figure 10: Comparison of scan patterns between simulation and experiment: (a) scan patterns in columns and (b) scan patterns in rows.

Table 2: Discrepancy of scan density and number of scan points between simulation and experimental data.

Inc. ang. (°)	Ang. resol. (°)	Number of scan points (pts)			Scan density (pts/cm^2)		
		Exp.	Sim.	Discrepancy (%)	Exp.	Sim.	Discrepancy (%)
0	0.036	269,736	271,314	0.58	71,03	68.52	3.53
	0.072	66,490	67,829	1.97	17,85	17.16	3.88
45	0.036	100,210	92,203	7.99	26,79	24.91	7.02
	0.072	24,614	23,070	6.27	6,71	6.33	5.57
Average	—	115,263	113,604	4.20	30.59	29.23	5.00

occurred at the case of incident angle of 45° and angular resolution of 0.072°. Here, the scan density (points/cm^2) refers to the number of scan points within an area of 1 cm × 1 cm. Figure 11 shows three selected areas for the comparison of scan density between the scan points from simulation and experiment. The discrepancy of scan density ranged from 3.53% to 7.02%, with an average discrepancy of 5%. Similar to the trend of number of scan points, the largest discrepancy was obtained at the case of incident angle of 45° and angular resolution of 0.072°. Based on these findings, it can be inferred that the simulated scan points closely resemble the experimental scan points, providing evidence for the effectiveness of the developed geometric model for simulation-based edge extraction assessment.

5. Evaluation of Edge Extraction Algorithms

5.1. Overview. For evaluation of the five edge extraction algorithms, a number of simulations and experimental tests were carried out. For evaluation, the corner points of the top surface were computed using the algorithms by determining the intersection points of the estimated edge lines. Figure 12 shows example results of edge line estimation and corner point extraction using the LSR 2 algorithm on the top surface and two side surfaces. A total of 44 corner points, including 28 corners from the outer border and 16 corners from shear pockets on the top surface, were used to evaluate the accuracy. For side surface, there are four outer boundary points and 16 corners from shear keys on the side surface. These corner points were utilized to calculate the discrepancies between the actual dimensions and the estimated top surface corners. Note that the actual corners serving as the reference points were measured using a measuring tape.

5.2. DQA Evaluation Results. Table 3 presents the accuracy of edge line estimation for both simulated and experimental scan points across different incident angles and angular resolutions. First, for simulation results, it shows that the LSR2 algorithm performs the best in corner extraction with an average discrepancy of 1.56 mm. This phenomenon indicates that the LSR 2 algorithm, which excludes mixed pixel scan points for edge line fitting, performs better than other algorithms that include mixed pixel scan points for edge line fitting. In addition, the results of the RANSAC

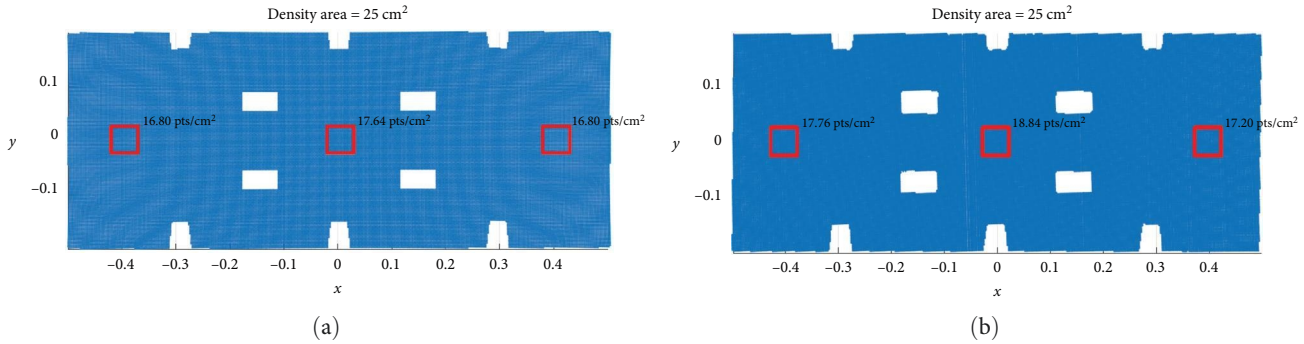

(a) (b)

Figure 11: Three selected areas for comparison of scan density between simulation and experiment: (a) simulation and (b) experiment.

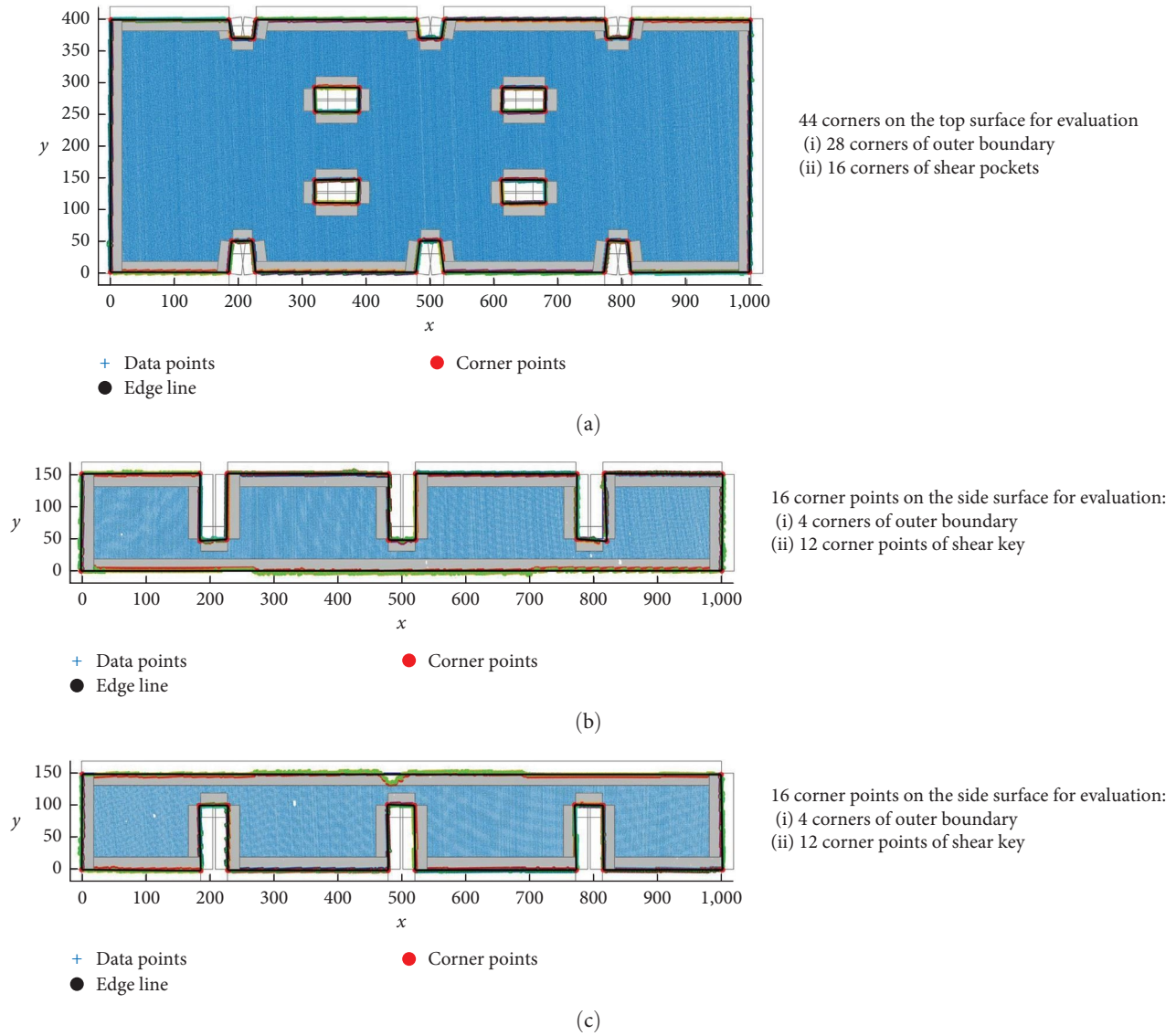

Figure 12: Results of corner point and edge line extraction: (a) the top surface; (b) the Side Surface 1; and (c) the Side Surface 2. Here, the visualized results are obtained from the LSR2 algorithm.

algorithm are affected by the input parameters required for the implementation of the algorithms. Specifically, the input parameters of the RANSAC algorithm for line fitting include (1) the minimum number of data points required for fitting, (2) the maximum number of iterations, and (3) the range of acceptable errors. In contrast, LSR algorithms require no input parameters. Therefore, the LSR algorithm is more robust to edge line estimation compared to the

Table 3: Edge line estimation accuracy of experimental scan points with varying incident angles and angular resolutions.

Dataset	Scan indicator Area	Idc. ang. (°)	Ang. resol (°)	Accuracy (mm) Vector-sum	LSR 1	LSR 2	RAN. 1	RAN. 2
Simulation	Outer corners	0	0.036	1.25	1.82	1.11	1.87	1.23
		—	0.072	1.57	1.86	0.80	3.22	2.88
		45	0.036	1.38	2.00	0.92	2.98	2.48
		—	0.072	3.41	2.86	2.24	5.53	5.68
	Shear pocket	0	0.036	0.73	2.10	1.79	1.90	1.62
		—	0.072	1.88	2.46	2.03	2.06	1.78
		45	0.036	1.35	2.14	1.72	2.24	1.85
		—	0.072	2.42	1.64	1.88	1.42	1.84
Ave.		—	—	1.75	2.11	1.56	2.65	2.42
Experiment	Outer corners	0	0.036	1.56	2.48	1.81	2.67	2.07
		—	0.072	3.09	3.93	2.62	4.47	3.74
		45	0.036	2.62	2.97	2.52	3.90	3.44
		—	0.072	5.39	5.19	4.43	6.88	6.39
	Shear pocket	0	0.036	1.65	2.40	2.10	2.74	2.45
		—	0.072	2.75	3.58	2.93	3.94	3.14
		45	0.036	2.05	2.80	2.35	3.05	2.59
		—	0.072	4.36	3.87	2.88	3.88	2.86
Ave.		—	—	2.93	3.40	2.71	3.94	3.33

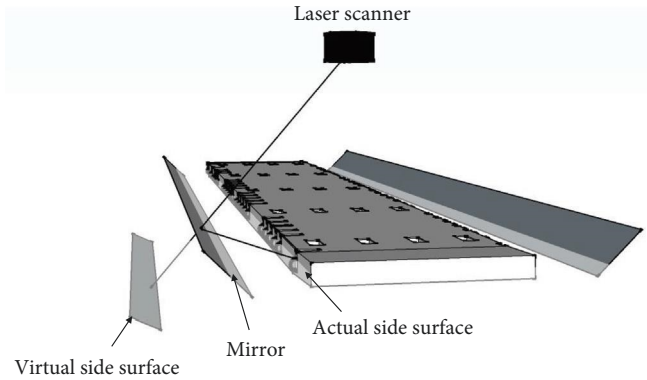

Figure 13: Generation of the simulated scan points on the side surfaces.

other algorithms. For the results of experiment, the edge line estimation accuracy varied from 1.56 to 6.88 mm, with an average DQA accuracy of 3.26 mm. Similar to the simulated scan points, the LSR2 algorithm provides the best DQA performance with an average discrepancy of 2.71 mm. In overall, a clear observation was found that the simulation results always showed better performance than the experimental results. This is because the simulated data set was generated under ideal conditions while actual scan data may include noise source.

The edge line estimation accuracy on the two side surfaces was also evaluated using simulated and experimental scan points. Figure 13 shows the generation of simulated scan points on the side surfaces. First, a virtual side surface that is symmetric to the actual side surface was generated due to the principle of mirror reflection. Subsequently, the scan points falling on the virtual side surface were simulated using the developed geometrical model. In this study, an incident angle of 0° was selected to evaluate the edge line extraction on the side surfaces because some edges of the side surfaces are occluded by the rebar under the incident angle of 45° as shown in Figure 14. The presence of rebar obstructs the laser scanner's visibility of the shear keys at larger incident angles, leading to less accurate DQA results. Therefore, it is necessary to adjust the incident angle on the side surfaces properly to avoid occlusions. Further investigation will be a future direction for study to address the occlusion issue, so further investigation is out of scope of this study. Table 4 shows the edge line estimation accuracy of the two side surfaces. The DQA accuracy of the simulated scan points ranged from 1.50 to 4.15 mm, with an average of 2.24 mm. The average edge line estimation accuracy from the experiment was 2.56 mm, which ranges from 1.34 to 5.05 mm. Similar to the top surface results, the simulation results always showed a better

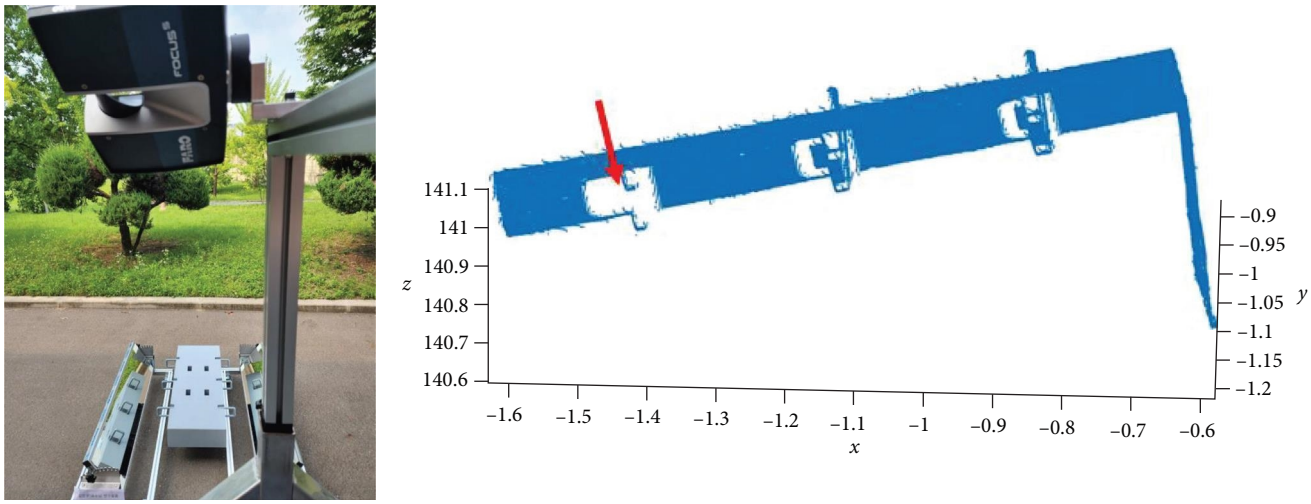

(a) (b)

Figure 14: Occlusion issue on the side surface caused by rebars under the incident angle of 45°: (a) experimental configuration under the incident angle of 45°; (b) the results of the occlusion issue on the side surface caused by rebar.

Table 4: Edge line estimation accuracy of simulated and experimental scan points with varying incident angles and angular resolutions for the two side surfaces.

Data set	Scan indicator Area	Ang. resol (°)	Accuracy (mm) Vector-sum	LSR 1	LSR 2	RAN. 1	RAN. 2
Simulation	Side surface 1	0.036	1.64	1.50	1.59	1.87	1.91
		0.072	2.02	2.35	2.54	3.71	3.95
	Side surface 2	0.036	1.83	1.22	1.33	1.56	1.81
		0.072	2.63	2.26	1.89	4.15	2.99
Average		—	2.03	1.83	1.87	2.82	2.67
Experiment	Side surface 1	0.036	1.97	1.80	1.98	2.27	2.35
		0.072	2.26	2.67	2.73	3.81	4.03
	Side surface 2	0.036	1.91	1.34	1.53	1.86	1.99
		0.072	2.72	2.40	2.07	5.05	4.49
Average		—	2.22	2.05	2.08	3.25	3.22

performance than the experimental results on the two side surfaces. In addition, it is observed from both the simulation and experiment that the LSR1 and LSR2 algorithms show better edge line estimation results than the other three algorithms.

6. Discussions

Further studies were conducted in order to provide better insights of the proposed approach, including (1) influencing factor analysis and (2) determination of optimal scan density for DQA.

6.1. Influencing Factor Analysis. In this section, an analysis was conducted to examine how scan parameters influence edge line estimation accuracy for the purpose of identifying an ideal scan configuration. In this study, two factors including (1) incident angle and (2) angular resolution were investigated. Figure 15 shows the effects of these two factors. There are three main observations from the analysis. First, the DQA accuracy of the shear pockets is more accurate than that of the outer corner points. This is because the incident angles of the inside corners located near the middle of the surface are relatively lower in comparison to the corners of the outer boundary. Second, all DQA accuracies of the shear pockets were below 3 mm, which were similar under different scan configurations. This is because shear pockets with rectangular shapes have relatively stable DQA results, which are not significantly influenced by the various angular resolutions and incident angles. Third, the DQA accuracy increased when the incident angle changed from 45° to 0°. This also explains why the combination of an incident angle of 0° and angular resolution of 0.036° yields higher DQA accuracy in most cases in Tables 2–4. These findings indicate that scan configurations characterized by a low incident angle and high angular resolution are likely to result in accurate DQA of PC slabs during the manufacturing process and construction stages. Therefore, it is recommended to select

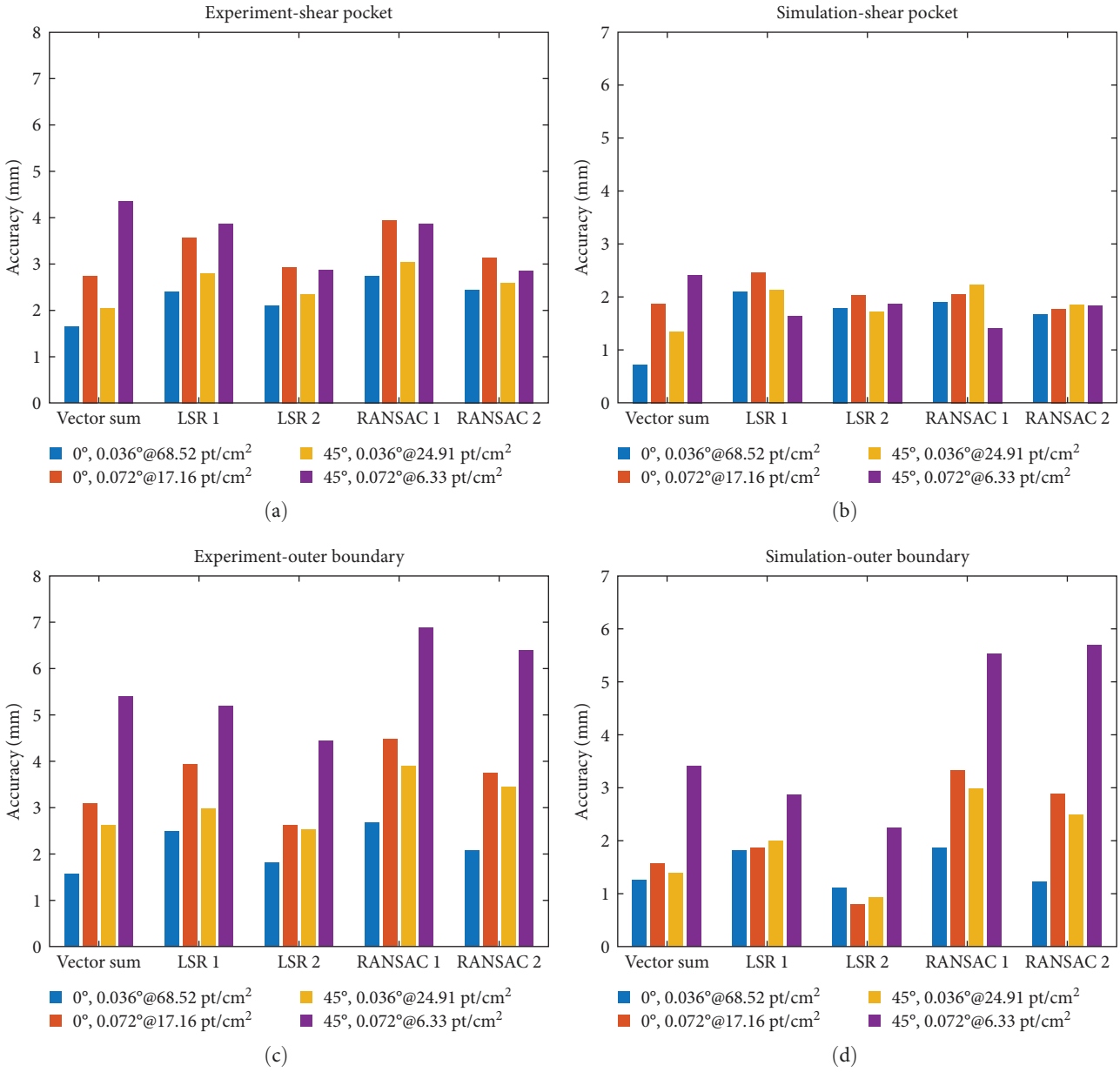

Figure 15: Edge line estimation accuracy on shear pocket and outer boundary using simulated scan points and experimental scan points: (a) Discrepancies of shear pocket in experimental scan points; (b) discrepancies of shear pocket in simulated scan points; (c) discrepancies of outer boundary in experimental scan points; (d) discrepancies of outer boundary discrepancies in simulated scan points.

lower incident angles and high angular resolutions for conducting the DQA of PC slabs.

6.2. Determination of Optimal Scan Density for DQA. The correlation between scan density and DQA accuracy was further investigated to determine an optimal scan density. Figure 16 shows the correlation results between scan dentistry and DQA accuracy. It shows that as scan density increases from 2.17 to 5 pts/cm^2, the corresponding DQA errors of the shear pocket decrease from 3.36 to 1.45 mm. When the scan density exceeds 5 pts/cm^2, the scan density made less influence on the DQA accuracy of the shear pocket. For outer boundary DQA, the positive correlation between the scan density and the DQA accuracy occurs when the scan density increases from 2.17 to 10 pts/cm^2. Therefore, 5 and 10 pts/cm^2 are selected as the optimal scan densities to guarantee accurate DQA of the shear pocket and outer boundary, respectively. In summary, it has been proven that the simulation-based evaluation method has the potential for determining optimal scan density for DQA of PC components. With respect to the selected scan density, the optimal scanning parameters can be determined using simulated scan points without actual scans, resulting in efficient scan configuration determination. Previous studies have investigated the correlation between scan density and dimensional accuracy for construction elements including MEP components [37] and rebars [38]. Although the optimal scan density can also be determined for performing

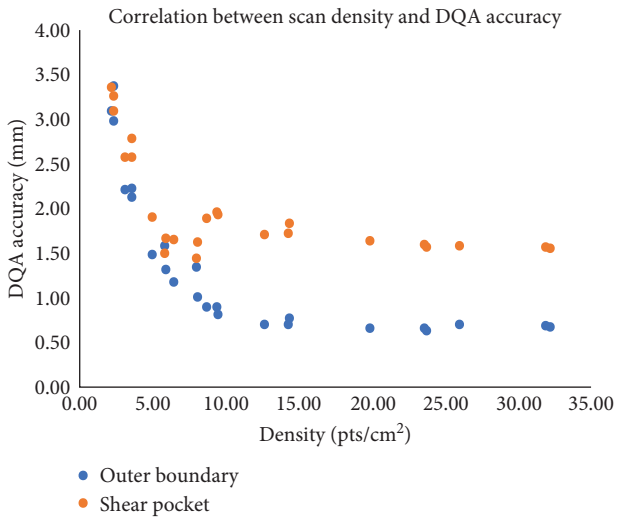

Figure 16: Correlation between scan dentistry and DQA accuracy.

DQA, these findings are investigated by conducting actual experiments, which is inefficient compared to the proposed simulated method.

7. Conclusions

This article presents a simulation-based DQA assessment approach to evaluate the performance of five edge extraction algorithms for the DQA of PC elements. For validation of the developed geometrical model for simulation, a comparison test was conducted on both the simulated and experimental scan points. The results showed that both the simulated and experimental scan points had a high similarity of more than 90% in terms of scan pattern, density, and the number of scan points, proving the effectiveness of the simulation-based evaluation method. A series of experimental and simulation tests were conducted to further evaluate the performance of the five edge line estimation algorithms. From the comparison, the LSR2 algorithm provides the best performance with an accuracy of 1.56 and 2.71 mm in simulated scan points and experimental scan points, respectively. As a result, the LSR 2 algorithm is identified as the optimal choice for ensuring precise DQA of PC elements. From the further investigation, it is recommended to (1) use lower incident angles and high angular resolutions for DQA of PC elements and (2) properly adjust the incident angle on the side surfaces to avoid occlusion. It is also noted that the simulation-based evaluation method does not require all combination of actual scanning with different scan parameters, which can significantly reduce scanning time. The contributions of this study are (1) development of the geometrical model and noise modeling based on actual scan data and (2) validation of simulated-based evaluation method of current existing edge line algorithms on the lab-scale PC slabs.

Nonetheless, the scope of this study is focused exclusively on five edge line extraction algorithms for PC slabs having planar surface. Additional research is necessary to assess the most suitable edge line estimation algorithms for curved and other shapes of PC components. Also note that previous studies have explored the impact of environmental factors, including humidity. As this study is focused on developing a simulation-based evaluation method, investigation on the effects of additional factors on the simulation based DQA evaluation method can be a future research direction. Moreover, as mentioned in Section 4, it is necessary to further investigate the mirror setup that properly avoids occlusions on the side surfaces.

Data Availability

The data used to support the findings can be obtained by contacting joekim@chungbuk.ac.kr.

Conflicts of Interest

The authors declare that they have no conflicts of interest.

Acknowledgments

This research was supported by four funding sources including the National R&D Project for Smart Construction Technology (Grant RS-2020-KAI156887) funded by the Korea Agency for Infrastructure Technology Advancement under the Ministry of Land, Infrastructure, and Transport and managed by the Korea Expressway Corporation; the National Research Foundation of Korea (NRF) grant funded by the Korean government (MSIT) (Grants 2019R1C1C1010662 and 2022R1A2C1005184); and the National Natural Science Foundation of China (Grant 523038211).

References

[1] M.-K. Kim, Q. Wang, and H. Li, "Non-contact sensing based geometric quality assessment of buildings and civil structures: a review," *Automation in Construction*, vol. 100, pp. 163–179, 2019.

[2] S. Wan, S. Guan, and Y. Tang, "Advancing bridge structural health monitoring: insights into knowledge-driven and data-driven approaches," *Journal of Data Science and Intelligent Systems*, 2023.

[3] Z. Wu, Y. Tang, B. Hong, B. Liang, and Y. Liu, "Enhanced precision in dam crack width measurement: leveraging advanced lightweight network identification for pixel-level accuracy," *International Journal of Intelligent Systems*, vol. 2023, Article ID 9940881, 16 pages, 2023.

[4] M. Nahangi, J. Yeung, C. T. Haas, S. Walbridge, and J. West, "Automated assembly discrepancy feedback using 3D imaging and forward kinematics," *Automation in Construction*, vol. 56, pp. 36–46, 2015.

[5] M. Nahangi and C. T. Haas, "Skeleton-based discrepancy feedback for automated realignment of industrial assemblies," *Automation in Construction*, vol. 61, pp. 147–161, 2016.

[6] J.-H. Chen, S.-C. Hsu, C.-L. Chen, H.-W. Tai, and T.-H. Wu, "Exploring the association rules of work activities for producing precast components," *Automation in Construction*, vol. 111, Article ID 103059, 2020.

[7] P. Rodríguez-Gonzálvez, M. Rodríguez-Martín, L. F. Ramos, and D. González-Aguilera, "3D reconstruction methods and quality assessment for visual inspection of welds," *Automation in Construction*, vol. 79, pp. 49–58, 2017.

[8] M. Rodríguez-Martín, P. Rodríguez-Gonzálvez, S. Lagüela, and D. González-Aguilera, "Macro-photogrammetry as a tool for the accurate measurement of three-dimensional misalignment in welding," *Automation in Construction*, vol. 71, pp. 189–197, 2016.

[9] Q. Wang, J. C. P. Cheng, and H. Sohn, "Automated estimation of reinforced precast concrete rebar positions using colored laser scan data," *Computer-Aided Civil and Infrastructure Engineering*, vol. 32, no. 9, pp. 787–802, 2017.

[10] R. Sacks, C. M. Eastman, and G. Lee, "Process model perspectives on management and engineering procedures in the precast/prestressed concrete industry," *Journal of Construction Engineering and Management*, vol. 130, no. 2, pp. 206–215, 2004.

[11] Y. Shahtaheri, C. Rausch, J. West, C. Haas, and M. Nahangi, "Managing risk in modular construction using dimensional and geometric tolerance strategies," *Automation in Construction*, vol. 83, pp. 303–315, 2017.

[12] B. M. Phares, G. A. Washer, D. D. Rolander, B. A. Graybeal, and M. Moore, "Routine highway bridge inspection condition documentation accuracy and reliability," *Journal of Bridge Engineering*, vol. 9, no. 4, pp. 403–413, 2004.

[13] C. Z. Li, R. Y. Zhong, F. Xue et al., "Integrating RFID and BIM technologies for mitigating risks and improving schedule performance of prefabricated house construction," *Journal of Cleaner Production*, vol. 165, pp. 1048–1062, 2017.

[14] P.-E. Josephson and Y. Hammarlund, "The causes and costs of defects in construction: a study of seven building projects," *Automation in Construction*, vol. 8, no. 6, pp. 681–687, 1999.

[15] P. W. Birkeland and L. J. Westhoff, "Dimensional tolerances in a tall concrete building," *Journal Proceedings*, vol. 68, no. 8, pp. 600–607, 1971.

[16] C. Brenner, "Building reconstruction from images and laser scanning," *International Journal of Applied Earth Observation and Geoinformation*, vol. 6, no. 3-4, pp. 187–198, 2005.

[17] E. P. Baltsavias, "A comparison between photogrammetry and laser scanning," *ISPRS Journal of Photogrammetry and Remote Sensing*, vol. 54, no. 2-3, pp. 83–94, 1999.

[18] H. Kwon, S. Jeon, J. Lee, and K. Jeong, "Development of a simulation model for supply chain management of precast concrete," *Korean Journal of Construction Engineering and Management*, vol. 22, pp. 86–98, 2021.

[19] S. Jo, J. G. Lee, and J. Choi, "A framework of automating inspection task generation for construction projects," *Korean Journal of Construction Engineering and Management*, vol. 24, pp. 40–50, 2023.

[20] S.-H. Kwon, J. S. Kim, and S.-H. Sim M. Kim, "Suitability analysis of non-contact sensing methods for precast concrete element flatness inspection," *Korean Journal of Construction Engineering and Management*, vol. 24, pp. 52–59, 2023.

[21] PCI, *Tolerance Manual for Precast and Prestressed Concrete Construction*, Precast/Prestressed Concrete Institute, 2000.

[22] ACI, "Identification and control of visible effects of consolidation on formed concrete surfaces," 1998.

[23] F. Li and M.-K. Kim, "Mirror-aided registration-free geometric quality inspection of planar-type prefabricated elements using terrestrial laser scanning," *Automation in Construction*, vol. 121, Article ID 103442, 2021.

[24] M. Kim, Q. Wang, J. Park, J. C. Cheng, H. Sohn, and C. Chang, "Automated dimensional quality assurance of full-scale precast concrete elements using laser scanning and BIM," *Automation in Construction*, vol. 72, pp. 102–114, 2016.

[25] F. Bosché, "Automated recognition of 3D CAD model objects in laser scans and calculation of as-built dimensions for dimensional compliance control in construction," *Advanced Engineering Informatics*, vol. 24, no. 1, pp. 107–118, 2010.

[26] F. Bosche, C. T. Haas, and B. Akinci, "Automated recognition of 3D CAD objects in site laser scans for project 3D status visualization and performance control," *Journal of Computing in Civil Engineering*, vol. 23, no. 6, pp. 311–318, 2009..

[27] L. Truong-Hong, D. F. Laefer, T. Hinks, and H. Carr, "Flying voxel method with delaunay triangulation criterion for façade/feature detection for computation," *Journal of Computing in Civil Engineering*, vol. 26, no. 6, pp. 691–707, 2012.

[28] L. Truong-Hong, D. F. Laefer, T. Hinks, and H. Carr, "Combining an angle criterion with voxelization and the flying voxel method in reconstructing building models from lidar data," *Computer-Aided Civil and Infrastructure Engineering*, vol. 28, no. 2, pp. 112–129, 2013.

[29] M. Cabaleiro, R. Lindenbergh, W. F. Gard, P. Arias, and J. W. G. van de Kuilen, "Algorithm for automatic detection and analysis of cracks in timber beams from lidar data," *Construction and Building Materials*, vol. 130, pp. 41–53, 2017.

[30] S. Yoon, Q. Wang, and H. Sohn, "Optimal placement of precast bridge deck slabs with respect to precast girders using 3D laser scanning," *Automation in Construction*, vol. 86, pp. 81–98, 2018.

[31] M.-K. Kim, H. Sohn, and C.-C. Chang, "Automated dimensional quality assessment of precast concrete panels using terrestrial laser scanning," *Automation in Construction*, vol. 45, pp. 163–177, 2014.

[32] C. Lu, H. Min, Z. Zhao, L. Zhu, D. Huang, and S. Yan, "Robust and efficient subspace segmentation via least squares regression," in *Computer Vision-ECCV 2012: 12th European Conference on Computer Vision*, pp. 347–360, Springer, Florence, Italy, Proceedings, Part VII 12, 2012.

[33] Q. Wang, H. Sohn, and J. C. P. Cheng, "Development of high-accuracy edge line estimation algorithms using terrestrial laser scanning," *Automation in Construction*, vol. 101, pp. 59–71, 2019.

[34] M. A. Fischler and R. C. Bolles, "Random sample consensus: a paradigm for model fitting with applications to image analysis and automated cartography," *Communications of the ACM*, vol. 24, no. 6, pp. 381–395, 1981.

[35] P. Tang, B. Akinci, and D. Huber, "Quantification of edge loss of laser scanned data at spatial discontinuities," *Automation in Construction*, vol. 18, no. 8, pp. 1070–1083, 2009.

[36] E. Schubert, J. Sander, M. Ester, H. P. Kriegel, and X. Xu, "DBSACN revisited, revisited: why and how you should (still) use DBSCAN," *ACM Transactions on Database Systems*, vol. 42, no. 3, pp. 1–21, 2017.

[37] Q. Wang, J. Li, X. Tang, and X. Zhang, "How data quality affects model quality in scan-to-BIM: a case study of MEP scenes," *Automation in Construction*, vol. 144, no. 1, Article ID 104598., 2022.

[38] F. Li, M. K. Kim, and D. E. Lee, "Geometrical model based scan planning approach for the classification of rebar diameters," *Automation in Construction*, vol. 130, Article ID 103848., 2021.